



An annually resolved record of Western European vegetation response to Younger Dryas cooling

Igor Obreht^{a,*}, Lars Wörmer^a, Achim Brauer^{b,c}, Jenny Wendt^a, Susanne Alfken^a, David De Vleeschouwer^d, Marcus Elvert^a, Kai-Uwe Hinrichs^a

^a Organic Geochemistry Group, MARUM – Center for Marine Environmental Sciences and Department of Geosciences, University of Bremen, Leobener Str. 8, 28359, Bremen, Germany

^b GFZ – German Research Centre for Geosciences, Section Climate Dynamics and Landscape Evolution, Telegrafenberg, 14473, Potsdam, Germany

^c Potsdam University, Department of Earth Sciences, Karl-Liebknecht-Str. 24/25, 14476, Potsdam, Germany

^d Paleoceanography Group, MARUM – Center for Marine Environmental Sciences and Department of Geosciences, University of Bremen, Leobener Str. 8, 28359, Bremen, Germany

ARTICLE INFO

Article history:

Received 17 December 2019

Received in revised form

24 January 2020

Accepted 24 January 2020

Available online xxx

Keywords:

Lateglacial

Paleoclimatology

Western Europe

Meerfelder Maar

High-resolution biomarkers

Fatty acids

FT-ICR-MS

Mass Spectrometry Imaging

ABSTRACT

The regional patterns and timing of the Younger Dryas cooling in the North Atlantic realm were complex and are mechanistically incompletely understood. To enhance understanding of regional climate patterns, we present molecular biomarker records at subannual to annual resolution by mass spectrometry imaging (MSI) of sediments from the Lake Meerfelder Maar covering the Allerød-Younger Dryas transition. These analyses are supported by conventional extraction-based molecular-isotopic analyses, which both validate the imaging results and constrain the sources of the target compounds. The targeted fatty acid biomarkers serve as a gauge of the response of the local aquatic and terrestrial ecosystem to climate change. Based on the comparison of our data with existing data from Meerfelder Maar, we analyse the short-term environmental evolution in Western Europe during the studied time interval and confirm the previously reported delayed hydrological response to Greenland cooling. However, despite a detected delay of Western European environmental change of ~135 years, our biomarker data show statistically significant correlation with deuterium excess in Greenland ice core at ~ annual resolution during this time-transgressive cooling. This suggests a coherent atmospheric forcing across the North Atlantic realm during this transition. We propose that Western European cooling was postponed due to major reorganization of the westerlies that were intermittently forcing warmer and wetter air masses from lower latitudes to Western Europe and thus resulted in delayed cooling relative to Greenland.

© 2020 The Authors. Published by Elsevier Ltd. This is an open access article under the CC BY-NC-ND license (<http://creativecommons.org/licenses/by-nc-nd/4.0/>).

1. Introduction

The last glacial cycle is characterized by repeated abrupt millennial-scale climate oscillations known as Dansgaard–Oeschger events (Clement and Peterson, 2008). The Younger Dryas (~12,900–11,700 years BP) was the most recent abrupt cooling event of these climatic oscillations, during which the interplay of radiative forcing, a weakening of the Atlantic Meridional Overturning Circulation, and changes in atmospheric circulation resulted in Northern Hemisphere cooling (Björck et al., 2002; Clement and Peterson, 2008; Isarin et al., 1998; Renssen et al., 2015;

Schenk et al., 2018). Unfortunately, global hydroclimate teleconnections and the precise timing of the abrupt cooling among different regions are considerably underexplored. An increasing number of studies have demonstrated a clear offset in cooling recorded in Greenland ice cores and environmental shift in European lake records with a delay of up to two centuries (Lohne et al., 2013; Muschitiello and Wohlfarth, 2015; Muschitiello et al., 2015; Rach et al., 2014). Recently, Naughton et al. (2019) related the observed ~170 year long time-transgressive environmental response of southwestern Iberia and Central Europe to the steady reduction of the mid-latitude westerlies. They suggested that this scenario was triggered by ice sheet melting and the beginning of the southward extension of the sea-ice in the northern North Atlantic and the Nordic Seas at the beginning of abrupt cooling recorded in Greenland, which regionally reduced deep convection

* Corresponding author.

E-mail address: iobreht@marum.de (I. Obreht).

and heat release. On the other hand, results from Muschitiello et al. (2015) suggest that persistent sea-ice growth in the Nordic and North Seas occurred only ~180 years after the onset of Greenland cooling, causing an expansion of the southwards migration of North Atlantic storm track (Brauer et al., 2008; Rach et al., 2014). Consequently, the mechanisms behind such time-transgressive climate evolution and regional climate teleconnections over the North Atlantic realm during the Allerød-Younger Dryas transition are not fully understood. A prominent factor limiting our understanding of these mechanisms is insufficient sampling resolution of lacustrine and marine proxy records to capture climatic variations at the scale of ~annual resolution as provided by the North Greenland Ice Core Project (NGRIP) (Steffensen et al., 2008; North Greenland Ice Core Project Members, 2004; Gkinis et al., 2014).

In order to address these limitations, we applied an ultra-high-resolution molecular stratigraphy approach (Alfken et al., 2019; Wörmer et al., 2014, 2019) on an exceptionally well-dated Meerfelder Maar (MFM) sediment section spanning the Allerød-Younger Dryas transition. MFM is a maar lake in the Eifel region in Western Europe (Fig. 1) that is continuously varved throughout the Younger Dryas cold period (Brauer et al., 1999a, 2008). Its chronology is based on precise varve counting and robust ^{14}C dating further controlled by the presence of tephra layers (Brauer et al., 1999a, 2008), where the appearance of the Vedde Ash tephra layer allows for precise synchronization with NGRIP records (Lane et al., 2013, 2015; Rach et al., 2014). Consequently, it presents an ideal archive for high-resolution climate reconstruction. However, obtaining high-resolution biomarker-based paleoclimate records using conventional methods still represents a challenge due to sample size limitations.

Recent advances in Mass Spectrometry Imaging (MSI) of

sediments have revealed a great potential for providing information on various system properties such as temperature, vegetation, and the ecology of aquatic primary producers with unprecedented resolution (Wörmer et al., 2014, 2019). MSI is a laser-based technique that collects mass spectra of organic compounds at μm -scale spatial resolution, allowing for detection and visualization of single biomarkers based on exact mass on intact sediment core sections, and the construction of molecular biomarker records at ultra-high temporal resolution. Following recent advances in sample preparation and data evaluation (Alfken et al., 2019; Wörmer et al., 2019), we used MSI to obtain detailed information on fatty acid distribution in the MFM sediment. The spatial resolution of 200 μm allows for one to several measurements within a single year (Fig. 2), thus retrieving annual to sub-annual signals throughout the most of the record. Consequently, this ultra-high-resolution biomarker approach provides novel and unique insights that have the potential to illuminate the sequence of events during abrupt climate changes in the past and paves the way for interrogating the mechanisms of such events and of high-frequency climate oscillations that are relevant on the human time scale. The goal of this study was to decipher changes of paleoenvironmental dynamics during the Allerød-Younger Dryas transition in Western Europe at unprecedented level of detail, with a special focus on the delayed response of Western Europe climate to abrupt cooling recorded in Greenland ice-cores (onset of Greenland Stadial 1).

2. Methods

2.1. Study site

Lake Meerfelder Maar (50°06'2.87" N and 6°45'27.13" E; Fig. 1)

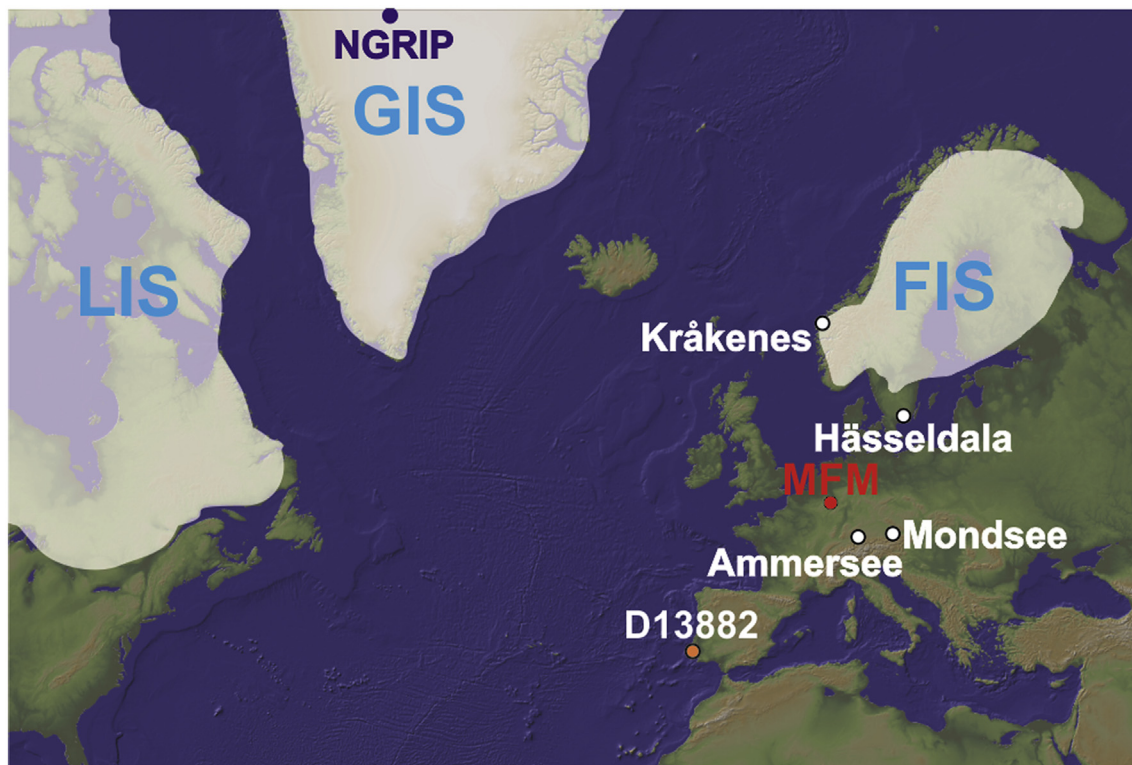


Fig. 1. Location of discussed records. Location of MFM is indicated with red point, where other Central and Northern Europe lake records are indicated with white points (Ammersee (Grafenstein et al., 1999), Mondsee (Lauterbach et al., 2011), Kråkenes (Bakke et al., 2009), Hässeldala (Muschitiello et al., 2015)). Core D13882 from Tagus mud patch (Naughton et al., 2019) is indicated with orange point. NGRIP (North Greenland Ice Core Project Members, 2004) is indicated with blue point. LIS refers to the Laurentide Ice Sheet, FIS refers to the Fennoscandia Ice Sheet, and GIS refers to the Greenland Ice sheet tentative distribution during the Younger Dryas (Dyke, 2004; Mangerud et al., 2016).

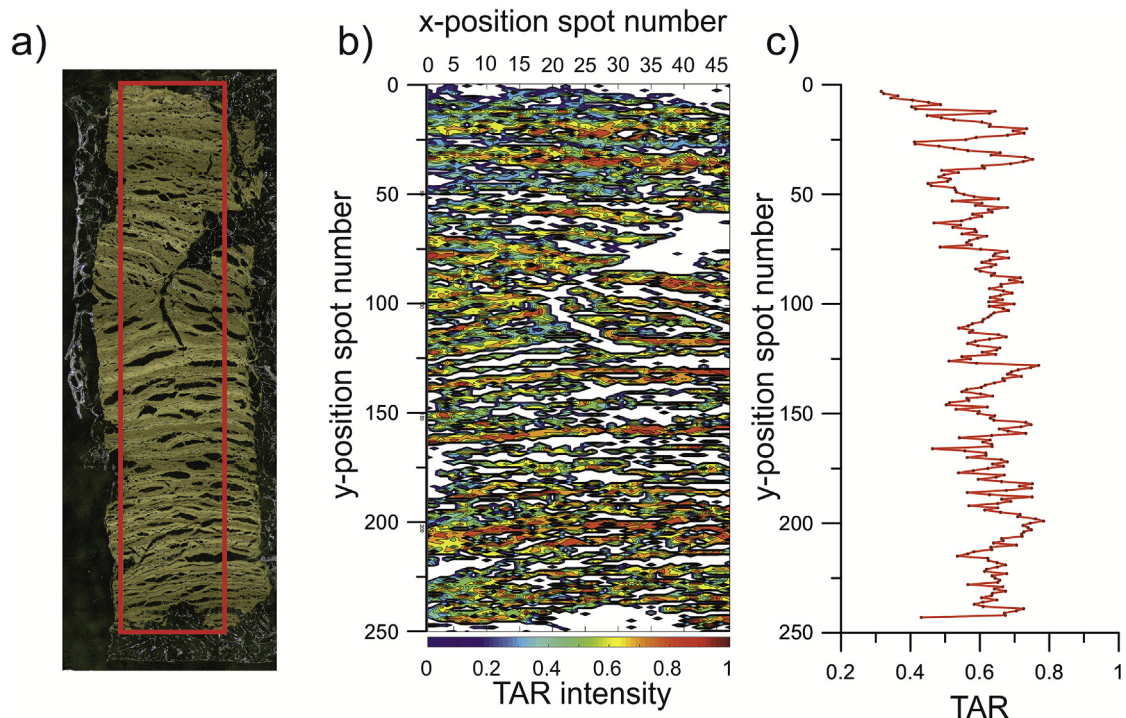


Fig. 2. An illustrative example of mass spectrometry imaging on a 5 cm sample section from core MFM09-A5-UR at a section depth of 23–28 cm. a) Image of the sample section, red rectangles indicate the area where MSI was performed. b) Spatial distribution of TAR values. c) Down-core TAR profile of horizontally averaged data points of the selected sample.

is a maar lake located in the Western-Eifel Volcanic Field (western Germany) at 336.5 m above sea level. The present lake level is 17 m and it covers one-third of the maar crater. Although MFM has a minimum age of 80,000 years (Rach et al., 2014; Zöller and Blanchard, 2009), the last ~15,000 years are the most intensively studied (Brauer et al., 1999b, 2008; Engels et al., 2016; Lehndorff et al., 2015; Martin-Puertas et al., 2012; Rach et al., 2014). MFM is particularly important for the period of the Younger Dryas since it is one of very few continuously varved lakes in Europe over this time interval (Brauer et al., 1999a, 1999b, 2008). The MFM09 cores were taken in 2009 by the German Research Centre for Geosciences Potsdam (GFZ) from the deepest part of the lake, using a UWITEC coring device (Martin-Puertas et al., 2012). Here we studied a 65 cm long section from core MFM09-A5-UR covering the Allerød-Younger Dryas transition. The onset of Younger Dryas is defined by a prominent change in biostratigraphy (Litt and Stebich, 1999), which coincides with an abrupt change in varve facies (Brauer et al., 2008), indicating a major vegetation change, an abrupt increase in storminess (Brauer et al., 2008), a decrease in lake level (Brauer et al., 2008) and shortenings of the growing season (Lücke and Brauer, 2004).

The age model is based on precise varve counting and 69 accelerator mass spectrometry ^{14}C dates for the entire record (Brauer et al., 1999a, 1999b, 2008). An initial age model of Lake Meerfelder Maar has been established by Brauer et al. (1999b) on a previously investigated composite profile, where a floating varve chronology based on varve counting was linked to an absolute timescale using the Ulmener-Maar tephra ($11,000 \pm 40$ years BP). The age model was further confirmed by Lane et al. (2013, 2015) when the Vedde Ash and other cryptotephra were discovered in the Meerfelder Maar sediments. This exceptional chronology provides an age model with the uncertainty of ± 40 years for the study interval. The previously established age-model has been

transferred to the new cores based on microscopic correlation of unequivocal marker varves.

2.2. Mass spectrometry imaging of sedimentary biomarkers

Data were obtained from core MFM09-A5-UR, where 35 cm were sampled above and 30 cm below Laacher See tephra using LL-channels. Sample preparation was performed according to Alfken et al. (2019). Samples were divided into 2.5–5 cm long subsamples and freeze-dried. To stabilize subsamples, they were embedded in a mixture of 5% gelatin and 1% sodium carboxymethyl cellulose and frozen. Each embedded subsample was sectioned into 60 μm and 100 μm thick slices using a cryomicrotome (Microm HM 505 E Cryostat, GMI, Ramsey, Minnesota, USA); the obtained slices were placed on indium-tin oxide-coated glass slides and dried in a desiccator. MSI was performed using a 7T solarix XR Fourier transform-ion cyclotron resonance-mass spectrometer (FT-ICR-MS) coupled to a matrix-assisted laser desorption/ionization (MALDI) source equipped with a Smartbeam II laser (Bruker Daltonik, Bremen, Germany). The selection of suitable proxies was limited to fatty acids, since other targeted compounds, such as alkenones, *n*-alkanes and glycerol dialkyl glycerol tetraethers, were undetectable or obtained in low quality. To enhance the sensitivity in the mass-to-charge ratio (m/z) range of the targeted fatty acids, data were acquired in continuous accumulation of selected ions mode (CASI) with m/z ranges at 355 ± 110 and 425 ± 55 . All data were acquired with 85% data reduction in fmsControl 2.1.0 (Bruker Daltonik). Analyses for detection of short and long-chain fatty acids were performed in CASI mode at $m/z 355 \pm 110$ on 100 μm slices, while analyses in the narrow CASI mode at $m/z 425 \pm 55$ were carried out on 60 μm slices for more precise detection of long-chain fatty acids. Fatty acids were detected as Na^+ -adducts. Data were calibrated to $\text{C}_{30}\text{H}_{50}$ for CASI mode at $m/z 425 \pm 55$, and to fatty acids $\text{C}_{16:0}$ and

C_{26:0} for CASI mode at m/z 355 ± 110 with a precision of ±0.005 Da in Data Analysis 4.4 (Bruker Daltonik). Afterwards, selected mass spectra in the region of interest were exported. The export routine generates a comma-separated file including spot position, m/z , intensity and signal to noise ratio (SNR) for every measured position. Exported data were further evaluated with Matlab R2017a (The MathWorks), where compounds of interest were identified according to a mass accuracy of ±0.005 Da. Since data were already reduced during acquisition (85%), only the most prominent peaks were recorded and an additional SNR threshold was not required. Proxy data were calculated with the corresponding intensities of the compounds of interest for each spot based on these filtered data. We used terrestrial to aquatic ratio (TAR) and average chain length (ACL) of fatty acids. To obtain a down-core profile, data were horizontally averaged and transformed into one data point. Data points were only generated when a minimum of 10 spots per horizon was available (Wörmer et al., 2019).

2.3. Gas chromatography-flame ionization detection and gas chromatography-isotope ratio mass spectrometry

20 samples were analyzed by gas chromatography-flame ionization detection (GC-FID) to crosscheck FT-ICR-MS data with the conventional method. Around 0.1 g of freeze-dried sediment samples were extracted using a modified Bligh and Dyer technique (Bligh and Dyer, 1959; Sturt et al., 2004; Wörmer et al., 2017). An aliquot of the total lipid extract was further separated into fractions containing neutral lipids and free fatty acids by aminopropyl solid phase extraction and elution with 8 ml of DCM/acetone (9:1) and 8 ml of 2% formic acid in DCM respectively. The extracts were dried under a stream of nitrogen and free fatty acids were derivatized with a solution of 500 µl 20% boron trifluoride in methanol and heated at 70 °C for 1 h to form fatty acid methyl esters (FAMES). After cooling, 500 µl of water was added to the mixture and FAMES were extracted three times with 500 µl of *n*-hexane from the water phase. Extracts were evaporated under a stream of nitrogen, redissolved in 100 µl *n*-hexane and analyzed via GC-FID. FAMES were detected using a ThermoFinnigan Trace GC-FID equipped with Restek Rxi-5ms capillary column (30 m × 0.25 mm ID). The GC-FID was programmed from an initial temperature of 60 °C (1 min isothermal) to 150 °C at a rate of 10 °C/min, and then to 310 °C at a rate of 4 °C/min. To measure stable carbon isotope ($\delta^{13}\text{C}$) values of the individual fatty acids, stable carbon isotopic compositions of individual FAMES were detected by gas chromatography-isotope ratio mass spectrometry (GC-IRMS) using a Thermo Fisher Scientific GC-Ultra connected to a GC-Isolink coupled via a con flow V to a Delta V plus. Stable carbon isotope values are reported in the delta-notation as $\delta^{13}\text{C}$ values relative to Vienna Pee Dee Belemnite (VPDB) with a precision of better than 1‰.

2.4. Correlation of chronologies from Meerfelder Maar, NGRIP and other records

Synchronization of different paleoclimate archives from different regions at a precision of only a few years is challenging and often not achieved due to dating uncertainties of independent chronologies. Maximal dating uncertainty at the Greenland Interstadial 1/Greenland Stadial 1 transition based on the NGRIP GICC05 age model is ±138 years (Rasmussen et al., 2006), while maximal dating uncertainty at the Allerød-Younger Dryas transition at MFM is ±40 years (Brauer et al., 2008). Consequently, a precise correlation of those records solely relying on independent dating is infeasible. However, a successful approach in synchronization of independent chronologies is tephrostratigraphy (Blockley et al.,

2014; Lane et al., 2013, 2015; Sirocko et al., 2013; Wulf et al., 2013). The Vedde Ash tephra layer has been identified in both, NGRIP and MFM records, allowing for precise correlation between these two records. At MFM, the Vedde Ash tephra layer was identified at 12,140 ± 40 years BP (Lane et al., 2013), while in the NGRIP ice-core it was dated at 12,171 ± 114 b2k (Rasmussen et al., 2006), which corresponds to 12,121 ± 114 years when converted to BP notation (as a difference in timescales where b2k refers to before 2000 AD, while BP refers to before 1950 AD). This indicates that despite larger absolute dating uncertainties, the difference between NGRIP and MFM chronologies around ~12,130 years BP is only 19 years. Considering the Vedde Ash as a robust tie point, we synchronized NGRIP and MFM chronologies at this datum to the precise year. Consequently, we converted the NGRIP record to the MFM time-scale, meaning that it is presented in BP notation scale and further adjusted for the 19 years offset. For the time interval from this tie point back to the start point of our study interval at ~13,400 years BP we applied a differential dating approach. Since both chronologies are based on annual layer counting, we can apply the mean counting uncertainty of ~1% determined for both chronologies for the ~1250-year time interval from the study interval to the Vedde Ash. This reduces the age uncertainties between these two records down to ±10 years at the Greenland Stadial 1/Younger Dryas onset. Therefore, we do not discuss leads and lags smaller than 20 years, which is the potential maximum offset between both chronologies during this particular interval.

Correlation of MFM to other records in Western Europe is feasible by using the widespread Laacher See tephra (LST) as an isochrone. In general, the majority of Western European paleoclimate records indicate that the onset of the Younger Dryas cold period followed ~200 years after the deposition of LST layer (Lotter et al., 1992; Riede et al., 2011; Sirocko et al., 2013; Wulf et al., 2013).

2.5 Sliding-window correlation analysis of time-series with non-zero autocorrelation

We adopted a sliding-window approach to calculate the Pearson correlation coefficient between NGRIP deuterium excess (d) (Steffensen et al., 2008) and TAR, as well as between NGRIP d and ACL. As all three time-series were serially correlated (nonzero autocorrelation), we could not use classical statistics to estimate the significance of the correlation. Instead, we used a nonparametric method to estimate the statistical significance of the correlation between TAR or ACL and NGRIP d that was developed by Ebisuzaki (1997). This method is implemented in the function *surrogateCor* (Baddouh et al., 2016), which is part of the *astrochron* package for R (Meyers et al., 2018). The TAR and ACL data-series were resampled on the sample grid of the NGRIP d data (i.e. 1-year resolution), using piecewise linear interpolation. Subsequently, the Pearson correlation coefficients were calculated using a sliding window approach. Sliding windows have a width of 160 data points (i.e. 160 years) and shift with increments of 10 data points (i.e. 10 years). Next, the *'surrogateCor'* function carried out the same correlation analyses for 10,000 Monte Carlo simulations, using phase-randomized surrogates. The surrogates were subject to the same interpolation process and compensated for the autocorrelation that characterizes both time-series (Ebisuzaki, 1997). The correlation coefficient of the data was then compared to the distribution of correlation coefficients obtained from the surrogates and allowed for the determination of a confidence level (p-value) for the correlation. We ran the sliding-window correlation analysis for five different age models, to assess the effect of age model uncertainties (see below) and shifted the ACL and TAR time-series by -10, -5, +5 and +10 years to reflect the uncertainty of the MFM - NGRIP tephra-based correlation.

3. Results and discussion

3.1. Data evaluation and proxy selection

The selection of suitable proxies to describe paleoenvironmental change in the MFM was limited by the fact that targeted paleothermometers, such as alkenones and glycerol dialkyl glycerol tetraethers, were undetectable by both conventional methods and MSI. *n*-Alkanes and fatty (*n*-alkanoic) acids are organic compounds well preserved in lake sediments and present one of the most widely used molecular proxies for the reconstruction of paleoclimate conditions (Conte and Weber, 2002; Hughen et al., 2004; Ishiwatari et al., 2006; Rach et al., 2014; Sachse et al., 2006). Since detection of *n*-alkanes using MSI is hampered by their very low ionization efficiency (Wörmer et al., 2019), we focused instead on fatty acids, a compound group that ionizes efficiently and provides analytically robust signals (Fig. 2). Fatty acids, however, present a challenging proxy for climate interpretation due to the existence of various potential sources and the lack of a straightforward relation to temperature and humidity (Huang et al., 2002, 2004; Meyers, 1997; Terwilliger et al., 2013). Despite these limitations, fatty acids can still be informative of changes of environmental conditions; particularly when corroborated by other proxy data they can provide information on the timing, but not magnitude, of vegetation response to climate. In this study, we combined ultra-high-resolution fatty acid data with previously published, more coarsely resolved, well-established sedimentological (Brauer et al., 1999a, 2008), pollen (Engels et al., 2015, 2016) and deuterium isotope data (Rach et al., 2014).

Long-chain fatty acids (C₂₄–C₂₈) exhibit an even-carbon-number predominance and are mainly, but not exclusively, synthesized by vascular plants as a component of leaf waxes (Bourbonniere and Meyers, 1996; Hughen et al., 2004; Meyers, 1997; Terwilliger et al., 2013). Especially in small maar lake systems like MFM, which are characterized by small catchments with steep and wind-sheltered crater walls, leaf-wax biomarkers such as fatty acids originate mostly from local sources (Rach et al., 2017). Moreover, biomarkers from terrestrial vascular plants must be transported from the source to the aquatic environment before deposition in sediments, potentially causing a temporal lag of the signal. Nevertheless, there is ample evidence that the residence time for plant waxes is rather short (Conte and Weber, 2002; Hughen et al., 2004), and in the case of MFM it is suggested that transfer time of leaf wax biomarkers from source to sediment is in the range of a season or a year (Rach et al., 2014, 2017).

Despite ionization of fatty acids by LDI-FTICR-MS being generally successful, the detection of low-abundance fatty acids was challenging. We observed a strong even-carbon-number predominance in fatty acids in MFM sediments, and consequently only low signal intensity of odd numbered ones. Accordingly, a higher number of high-quality data points was obtained when only even-numbered fatty acids (C_{24:0}, C_{26:0}, C_{28:0}) were included in the calculated ratios. Inclusion of odd-numbered fatty acids would remarkably decrease the robustness of data within the down-core profile and significantly decrease resolution. Therefore, we only used even-carbon-numbered fatty acids and defined ACL as:

$$ACL = (24 * C_{24:0} + 26 * C_{26:0} + 28 * C_{28:0}) / (C_{24:0} + C_{26:0} + C_{28:0}) \quad (1)$$

Validation of FT-ICR-MS data by GC-FID analyses is presented in Fig. 3. ACL data by FT-ICR-MS ranged from ~25.9 to 26.7, while GC-FID data ranged from ~25.9 to 26.3. Although the lower amplitude of GC-FID data is expected due to the much lower resolution, the absolute values of GC-FID and smoothed FT-ICR-MS data (mean

running average of 50 data points; Fig. 3) show a consistent positive offset in a range of ~0.25 units. This deviation is acceptable considering the use of different instruments and detector types, and specific parameter settings of the FT-ICR-MS (e.g. time of flight) that may provide a bias towards higher *m/z* values. Importantly, since absolute ACL values cannot be converted into a physical property such as temperature, we discuss only relative trends, and only the internal consistency of the dataset is relevant.

ACL time series of fatty acids are sensitive to variation in leaf wax composition as a consequence of environmental and climate change (Bush and McInerney, 2015; Hughen et al., 2004; Ishiwatari et al., 2006; Sepúlveda et al., 2009). In the Northern Hemisphere mid-latitudes ACL is mostly controlled by growing season temperature and humidity, although its dependence on the change in the type of vegetation has been reported as well (Bush and McInerney, 2015; Sachse et al., 2006). With changing temperature, wax-producing plants alter their leaf epicuticular wax composition to maintain its moisture balance and protect leaf membranes. Terrestrial vascular plants synthesize shorter-chain wax lipids in colder and dryer periods than in warmer and wetter periods (Bush and McInerney, 2015; Gagosian and Peltzer, 1986).

In contrast to long-chain fatty acids, most of the shorter-chain C_{14:0} to C_{18:0} fatty acids originate from aquatic sources (e.g. Bourbonniere and Meyers, 1996; Hou et al., 2006; Huang et al., 2002; Hughen et al., 2004). Therefore, a ratio between both compound groups is informative of the relative contribution of terrestrial and aquatic organic matter. We have generated three different terrestrial to aquatic ratios (Fig. 4). The TAR among saturated even-numbered C_{24:0}, C_{26:0} and C_{28:0} versus C_{14:0} and C_{16:0} fatty acids is commonly used (Bourbonniere and Meyers, 1996):

$$TAR_{24-28/14-16} = (C_{24} + C_{26} + C_{28}) / (C_{24} + C_{26} + C_{28} + C_{14} + C_{16}) \quad (2)$$

However, the yield of successful mass spectra by simultaneous MALDI analysis of five different compounds is lower than for ratios based on fewer fatty acids, which negatively impacts the data quality (Fig. 4 and Supplementary Fig. S1). Consequently, we generated TAR from the most abundant compounds in these two groups, namely the C_{16:0} fatty acid as an aquatic indicator and C_{26:0} fatty acid as a terrestrial indicator:

$$TAR = C_{26} / (C_{26} + C_{16}) \quad (3)$$

Both TARs provide records with highly similar trends ($R^2 = 0.9$), but TAR_(24-28/14-16) has a significantly lower yield of data points (Supplementary Fig. S1), as well as lower robustness of valid horizontally averaged data points (Fig. 4). Since both TARs are based on long-chain fatty acids influenced by the contribution of aquatic sources (see discussion in following chapter), we also present TAR based on the C_{24:0} fatty acid as an indicator of a terrestrial contribution without addition from aquatic sources (see discussion in following chapter) relative to the C_{16:0} fatty acid:

$$TAR_{24/16} = C_{24} / (C_{24} + C_{16}) \quad (4)$$

In general, TAR_{24/16} is highly correlated to both TAR_{24-28/14-16} ($R^2 = 0.77$) and TAR_{26/16} ($R^2 = 0.73$). Despite some deviations in presented TARs, those differences do not affect the overall trend discussed in the manuscript. In the rest of the manuscript the focus is on TAR based on C_{26:0} and C_{16:0} since it provides the highest quality data-set, but we highlight that TAR_{24/16} could be more representative due to solely terrestrial source of C_{24:0} (see discussion in following chapter).

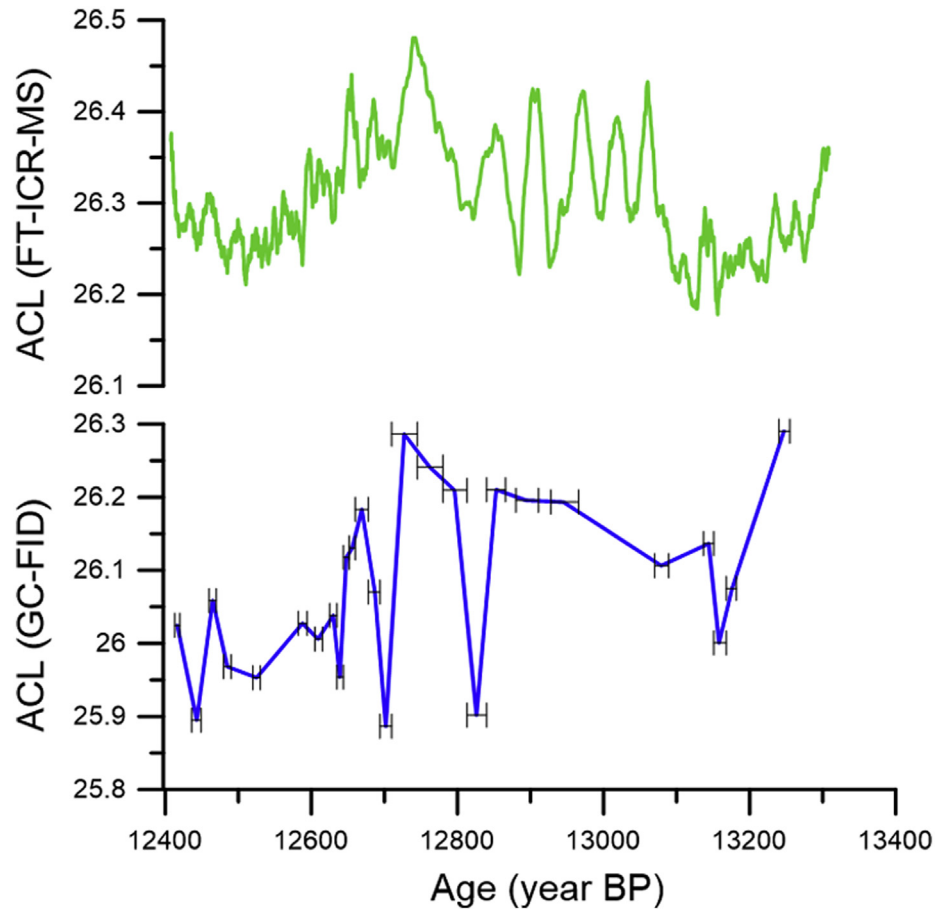


Fig. 3. Validation of data generated by FT-ICR-MS compared to conventional extraction based GC-FID data. Average chain length of saturated $C_{24:0}$, $C_{26:0}$ and $C_{28:0}$ fatty acids (ACL) data generated by FT-ICR-MS, here presented as moving average of 50 data points (green line) to smooth the high-frequency variability, and its comparison with GC-FID data (blue line). Bars in GC-FID data indicate the time interval covered by each sample.

3.2. Evaluation of alternative sources of fatty acids

Fatty acids are widely used paleoenvironmental proxies (Huang et al., 2002, 2004; Hughen et al., 2004; Ishiwatari et al., 2006; Meyers, 1997; Terwilliger et al., 2013), where long chain-fatty acids are suggested to be mostly synthesized by terrestrial vascular plants (Bourbonniere and Meyers, 1996; Hughen et al., 2004; Meyers, 1997). To verify the sources of the fatty acids targeted by MSI and thus validate their use for paleoclimate reconstruction, we measured $\delta^{13}C$ values of the individual fatty acids. Terrestrial C_3 plants exhibit a large range of $\delta^{13}C$ values from -20 to -37% (average $\sim -27\%$) (Kohn, 2010; O'Leary, 1988), mostly depending on the type of vegetation and aridity as a consequence of mean growing season temperature and precipitation. However, in our record $C_{26:0}$ and $C_{28:0}$ fatty acids have more negative $\delta^{13}C$ values than reported for terrestrial vegetation, in particular between 13,000 and 12,700 years BP (up to $\sim -43\%$; Fig. 5 and Supplementary Table 1). It is unlikely that such negative values are purely sourced by terrestrial plants. Such values rather indicate a contribution of $C_{26:0}$ and $C_{28:0}$ fatty acids from biological sources that utilize a ^{13}C -depleted carbon substrate for growth. The most plausible source are microbial communities that metabolize methane (Summons et al., 1994), which is characterized by extremely negative $\delta^{13}C$ in a range from -50% to -110% (Whiticar, 1999). In fact, the $\delta^{13}C$ value of bishomohopanoic acid ($\delta^{13}C_{BA}$), a general biomarker indicative of bacterial biomass (Bechtel and Schubert, 2009; Grimalt et al., 1991; Woszczyk et al., 2011),

shows $\delta^{13}C$ values from $\sim -52\%$ to -72% over the whole studied period (Fig. 5 and Supplementary Table 1), strongly suggesting the contribution of methanotrophic bacteria (Hinrichs et al., 2003; Summons et al., 1994). Anoxic bottom water and thus conditions conducive to methanogenesis are indicated by the deposition of varved sediments. In shallower oxygenated waters such conditions would support microbial methane oxidation by methanotrophic bacteria, which are known sources of ^{13}C -depleted hopanoids (Hinrichs et al., 2003). We therefore suggest that a fraction of $C_{26:0}$ and $C_{28:0}$ fatty acids with enhanced ^{13}C -depletion is also derived from methanotrophic bacteria. While they are not known to produce these compounds as constituents of the phospholipid membrane (Bodelier et al., 2009; Bowman et al., 1991), lipopolysaccharide-bound, hydroxylated derivatives of C_{26} , C_{28} and C_{30} fatty acids have been identified in considerable quantities in Type II methanotrophs (Bowman et al., 1991). Moreover, unusually ^{13}C -depleted C_{26} , C_{28} and C_{30} fatty acids have been observed in surficial sediments of the Santa Monica Basin, where they were assigned to microbial sources (Gong and Hollander, 1997).

A contribution of $C_{26:0}$ and $C_{28:0}$ fatty acids, but not $C_{24:0}$ or $C_{16:0}$, from a methanotrophic microbial source would potentially lead to increases in both TAR and ACL. To assess the influence of methanotrophic microbial sources to the time-series of ACL, we performed an end-member mixing analysis on $\delta^{13}C$ and GC-FID based ACL data (Supplementary discussion) that resulted in the definition of ACL from terrestrial sources (ACL_{terr}; Fig. 5), which we consider to have marginal influence from methanotrophic microbial sources. A

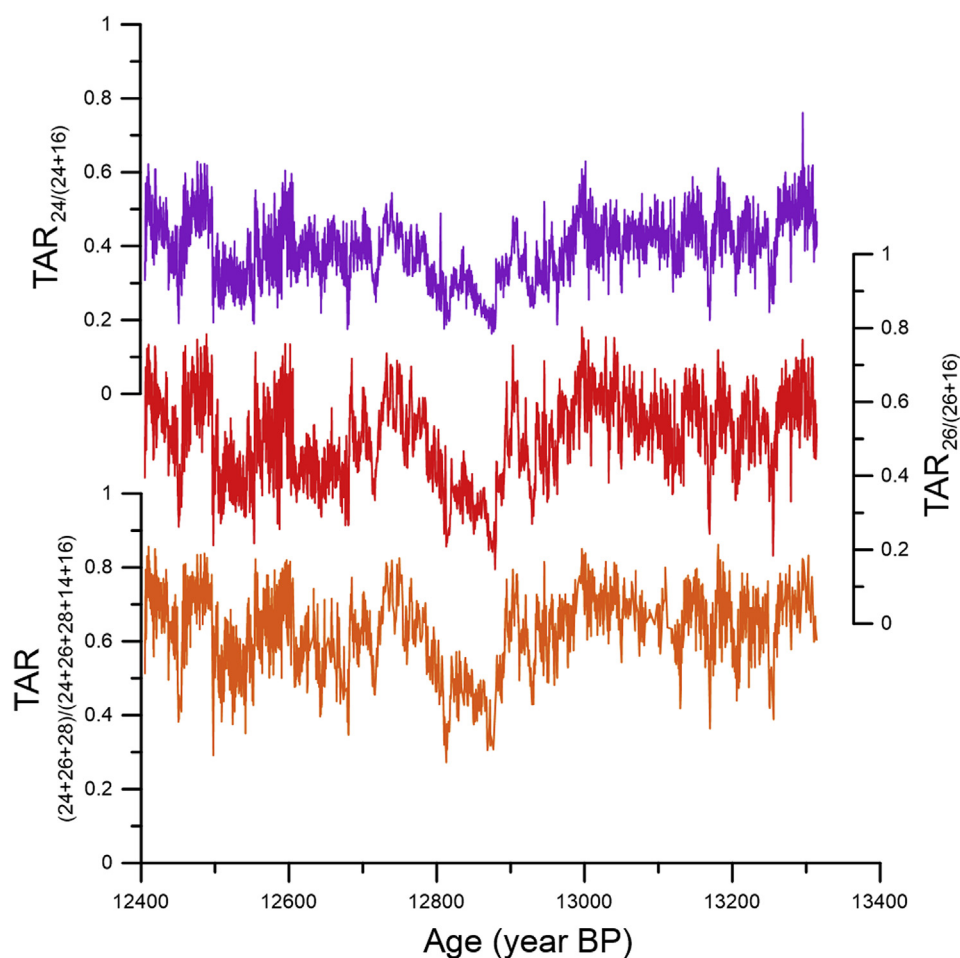


Fig. 4. Comparison among different terrestrial to aquatic ratios. Down-core profiles of $TAR_{26/(26+16)}$ (red line), $TAR_{24/(24+16)}$ and $TAR_{(24+26+28)/(24+26+28+14+16)}$ (dark red). From a total of 3521 horizons, 3461 were considered as robust for $TAR_{26/(26+16)}$, 3336 for $TAR_{24/(24+16)}$, and 2681 for $TAR_{(24+26+28)/(24+26+28+14+16)}$.

great similarity in general trends of ACL_{terr} and ACL demonstrates that the contribution from methanotrophic microbial sources has a relatively minor impact on the general longer-term ACL variations (Fig. 5). Considering that the ACL of higher plants increase with temperature in mid-latitudes (Bush and McInerney, 2015; Sachse et al., 2006), time periods characterized by an increase in ACL_{terr} and decrease in $\delta^{13}C_{BA}$ could be interpreted as periods of increasing temperature and methane oxidation, as increased temperature is expected to accelerate rates of methane production in sedimentary environments (Gu et al., 2011) (Fig. 5). This is a reasonable assumption since in modern European lake sediments methane production and temperature are directly linked (Bergström et al., 2007; Kankaala et al., 2005; Xing et al., 2005) and methane turnover intensities are stimulated during periods of temperature increase as a result of high primary productivity, as observed in e.g. thermokarst lake in Arctic Alaska (Elvert et al., 2016). Accordingly, increase in the contribution of methanotrophy-derived fatty acids due to increase in methane turnover would amplify the concurrent response of terrestrial vegetation to temperature, solidifying the relation in ACL time-series. On the other hand, non-methanotrophic heterotrophic microbes, such as bacteria, algae and fungi, are not considered to produce $> C_{24:0}$ fatty acids, but cannot be ruled out as additional possible contributors. However, $\delta^{13}C_{16}$ values representative of such aquatic sources exhibits generally more positive values than $\delta^{13}C$ of long-chained fatty acids (Fig. 5), suggesting that non-methanotrophic aquatic sources are

not a dominant contributors to long-chain fatty acids ($>C_{24}$).

3.3. Western Europe climate during the late Allerød and early Younger Dryas

In Fig. 6, we present annually to subannually resolved ACL and TAR records from the MFM during the late Allerød and early Younger Dryas, spanning a time interval from $13,315 \pm 40$ to $12,405 \pm 40$ years BP. Both ACL and TAR exhibit a gradual decrease over the first ~50 years of the studied period. ACL afterwards remains low over ~200 years, before changing to a more cyclic pattern from $13,100 \pm 40$ years BP until the deposition of the LST. TAR gradually increase between $\sim 13,100 \pm 40$ and $13,000 \pm 40$ years BP, while after $13,000 \pm 40$ years BP a decreasing trend is observed. This decrease in TAR likely reflects a decrease in terrestrial runoff due to a decrease in precipitation, as suggested by decreasing sedimentation rates. Spectral analyses of detrended TAR and ACL time-series (Supplementary Figs. S2 and S3) reveal a significant cyclicity of ~60 years in this time period, indicating a possible sensitivity to decadal oscillations in atmospheric systems. In this time interval, ACL seems to exhibit a similar variability in general trends as pollen accumulation rates (PAR) (Fig. 6), a proxy for the intensity of pollen production that is dependent on the amount of vegetation and temperature (Engels et al., 2015, 2016). This observation additionally supports our assessment of ACL primarily recording a signal from terrestrial higher plants.

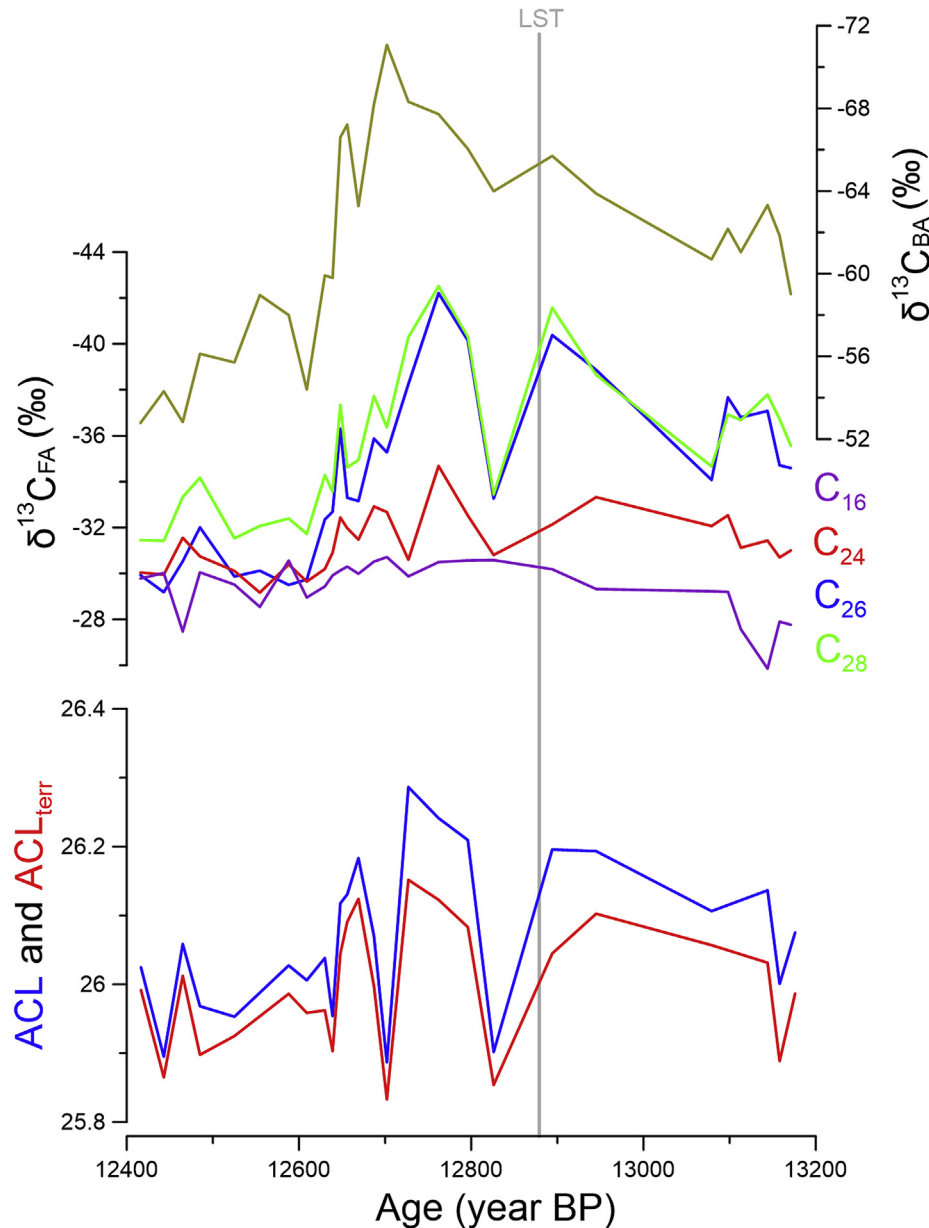


Fig. 5. Down-core profile comparison of stable carbon isotopes ($\delta^{13}\text{C}$) from individual fatty acids and bishomohopanoic acid with average chain length of fatty acids. Above: $\delta^{13}\text{C}$ values of bishomohopanoic acid ($\delta^{13}\text{C}_{\text{BA}}$; olive), $\delta^{13}\text{C}$ values of fatty acids ($\delta^{13}\text{C}_{\text{FA}}$) for $\text{C}_{16:0}$ (purple), $\text{C}_{24:0}$ (red), $\text{C}_{26:0}$ (blue) and $\text{C}_{28:0}$ (green). Below: comparison of ACL (blue) and corrected ACL for terrestrial input only (ACL_{terr} ; red; see Chapter 3.2 for more details). Note that $\delta^{13}\text{C}$ values are presented on a reversed scale.

ACL and TAR exhibit a prominent decrease in values ~20 years prior to LST deposition (Fig. 6), a feature also captured by pollen accumulation rates (Engels et al., 2015, 2016). Following deposition of the LST at $12,880 \pm 40$ years BP had a strong impact on regional climate and devastating influence on vegetation that persisted for at least 20 years (Engels et al., 2015). Consequently, a period of a few decades after the LST deposition, which was associated with low ACL, TAR and PAR (Fig. 6), as well as an increase in *Poaceae* species (Engels et al., 2015) (Fig. 7), cannot be solely related to climate forcing but rather represent local influence of tephra on vegetation, followed by vegetation recovery. A vegetation recovery of most species is considered to occur within ~20 years (Engels et al., 2016). Consequently, the continuous increase in ACL, TAR and PAR (Engels et al., 2015, 2016) that is evident until $12,730 \pm 40$ years BP, and particularly expressed after $12,800 \pm 40$ years BP

(Fig. 6), presumably represents a vegetation response to a progressive increase in temperature and humidity over the growing season. Similarities between ACL and $\delta^{18}\text{O}$ -based temperature records from Ammersee (Grafenstein et al., 1999) and Mondsee (Lauterbach et al., 2011) lakes also support milder summers in the wider region of Western Europe in this period (Fig. 6).

From $12,730 \pm 40$ years BP until the onset of the Younger Dryas in Western Europe defined by the change in biostratigraphy at $12,680 \pm 40$ years BP (Litt and Stebich, 1999), a notable decrease in ACL and TAR is observed indicating severe environmental changes, presumably related to decrease in temperature and humidity during the main growing season. This consistent trend of lower values is supported by lower pollen production (Engels et al., 2016) (decrease in PAR; Fig. 6), as well as a decrease in *Betula* and *Pinus* taxa in this period (Engels et al., 2016) (Fig. 7). Aridification is also

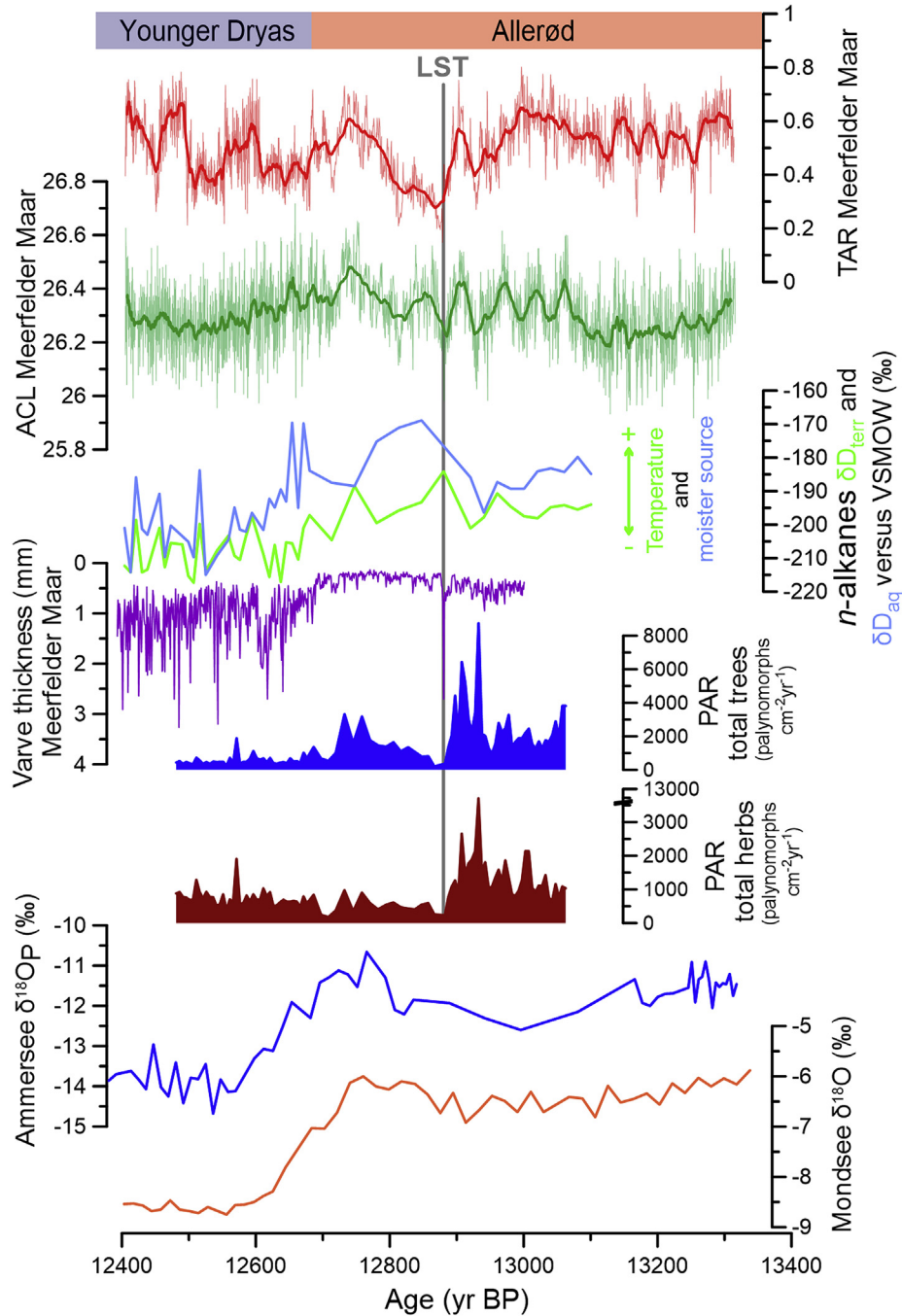


Fig. 6. Paleoclimate proxy data from Meerfelder Maar and temperature records from other European lakes. From top: TAR (red line; bold red line represents a moving average of 50 data points) and ACL (green line; bold green line represent a moving average of 50 data points), hydrogen isotopes of terrestrial C_{29} (δD_{terr} ; green line – indicator of temperature and moisture source) and aquatic C_{23} (δD_{aq} ; light blue line – indicator of moisture source) n -alkanes (Rach et al., 2014), varve thickness (purple line; Brauer et al., 2008), total pollen accumulation rates (PAR) for trees (blue fill; Engels et al., 2016) and herbs (dark red fill; Engels et al., 2016) from Meerfelder Maar compared with $\delta^{18}O_p$ from Ammersee (blue line; Grafenstein et al., 1999) and $\delta^{18}O$ from Mondsee (orange line; Lauterbach et al., 2011). Grey line refers to the Laacher See tephra (LST) layer in the Meerfelder Maar sediment. Note that the extremely high PAR values at 12,932 are probably related to methodological issues, rather than a true increase in pollen production (Engels et al., 2015).

consistent with the hydrogen isotope composition of lipid biomarkers from MFM, where the start of a long-term decrease in values indicates a major environmental and hydrological change in Western Europe (Rach et al., 2014) (Fig. 6).

With the onset of the Younger Dryas in Western Europe at $12,680 \pm 40$ years BP (Brauer et al., 2008; Litt and Stebich, 1999), ACL and TAR show an increase in the high-frequency band variability (Fig. 6). Although this can be partly explained by increase in

seasonality, as suggested by data and modelling studies (Björck et al., 2002; Denton et al., 2005; Isarin et al., 1998; Kelly et al., 2008; Schenk et al., 2018), we argue that this is rather a consequence of increased temporal resolution. With the onset of the Younger Dryas, varve thickness increases from values typically below 0.5 mm (providing 1–2 data points per year) to values generally higher than 0.5 mm (providing from 3 to 16 data points per year, depending on varve thickness; see Fig. 6), resulting in a

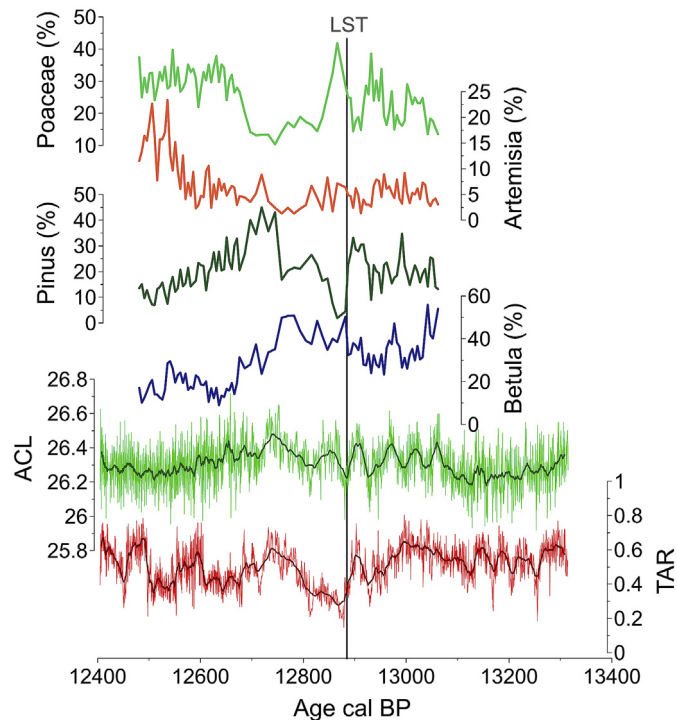


Fig. 7. Comparison of TAR, ACL and pollen data (Engels et al., 2016) from Meerfelder Maar. The pollen samples are expressed as percentages of the total pollen sum, and include pollen from four most abundant taxa (from top to bottom in the following order): *Poaceae*, *Artemisia*, *Pinus* and *Betula*. ACL and TAR are also presented as moving average of 50 data points (thick lines). LST is indicated with a black line.

shift from ~annual resolution in the late Allerød to subannual/seasonal resolution in the Younger Dryas. We also observed that after $12,600 \pm 40$ years BP TAR indicates alternating periods of abrupt increase and decrease in values, suggesting strong variability in productivity. Since the varve thickness slightly decreases from $\sim 12,610 \pm 40$ to $12,570 \pm 40$ years BP, higher TAR rather represents decrease in aquatic productivity than increase in runoff and terrestrial vegetation productivity in this period.

3.4. The time-transgressive onset of the Younger Dryas in the North Atlantic realm

The onset of abrupt cooling in Greenland defined as Greenland Stadial 1 (GS-1) began with abrupt reorganization in polar atmospheric circulation best recorded in NGRIP deuterium excess (d) record (Steffensen et al., 2008), the proxy for Greenland moisture origin. By synchronization of NGRIP and MFM chronologies applying differential dating approach and mean counting uncertainty, it can be assumed that the onset of GS-1 happened about 15 ± 10 years after the LST deposition (Fig. 8). Since the Laacher See volcanic eruption had a strong local influence on Western European vegetation over at least 20 years, establishing clear teleconnections between Western Europe and Greenland exactly at the onset of GS-1 is challenging. However, the following period of ~135 years after the onset of GS-1, which is characterized by prominent cooling recorded in NGRIP $\delta^{18}\text{O}$, is coeval with a progressive increase in ACL and TAR and consequently with milder climatic conditions in Western Europe (Fig. 8). We highlight that our biomarker proxies mainly record a climatic signal representative of the growing season, while data and model simulations (Björck et al., 2002; Denton et al., 2005; Isarin et al., 1998; Kelly et al., 2008; Schenk et al., 2018) suggest that the Younger Dryas cooling in Western Europe was

majorly controlled by winter cooling. Accordingly, the biomarker proxy records over the period of the time-transgressive cooling may be explained by suppressed cooling over the growing season in Western Europe, but contemporaneous winter cooling cannot be ruled out. Moreover, a decrease in ACL and TAR at the onset of the Younger Dryas is not necessarily related to significant cooling during the growing season, but can also be explained by shortening of the main growing period, which would be in agreement with previous studies (Lücke and Brauer, 2004).

We further examined temporal relationships of our ~ annually resolved ACL and TAR records to the NGRIP d record for the studied time period (Fig. 9). Through sliding-window correlation analysis (see Methods), we demonstrate that ACL and TAR records exhibit a statistically significant correlation to NGRIP d that is limited only to the time interval between the onset of GS-1 and delayed establishment of a stadial climate in Western Europe. The correlation between ACL and TAR with NGRIP d between $12,890 \pm 40$ and $12,730 \pm 40$ years BP exceeds the 95% confidence level using the above-presented chronology (Fig. 9). The correlation remains robust when age-model uncertainties of ± 10 years are considered, as correlation coefficients even exceed the 99% confidence level when we shift the age-model by +5 and +10 years (Fig. 9). Since the NGRIP d is a proxy of Greenland moisture origin (Masson-Delmotte et al., 2005; Steffensen et al., 2008), where higher or lower d values indicate a more distal south-westwards or more proximal north-eastward precipitation moisture source (Masson-Delmotte et al., 2005; Pfahl and Sodemann, 2014), respectively, an observed correlation on the ~annual to decadal-scale indicates a close link between changes in Greenland precipitation moisture source areas and Western Europe climate between ~12,880 and 12,730 years BP.

To explain the mechanisms of how changes in ACL and TAR are connected to changes in NGRIP d on an annual to multi-annual scale, it is important to note that d from Greenland ice-cores is strongly controlled by the temperature of the source area (Masson-Delmotte et al., 2005; Sánchez Goñi et al., 2009). The large increase in d values in Greenland ice with the onset of GS-1 indicates a south-westwards shift towards warmer moisture source areas (Masson-Delmotte et al., 2005). This implies that with the onset of Greenland cooling and following increase in sea-ice, the mid-latitude North Atlantic became much colder and did not provide much moisture to Greenland. Evaporation was restricted to subtropical and tropical locations, providing precipitation in Greenland largely in summer (Masson-Delmotte et al., 2005; Sánchez Goñi et al., 2009). Consequently, a progressive increase in NGRIP d after the abrupt increase at the onset of GS-1 is indicative of progressive shift in moisture source area from the mid-latitude North Atlantic realm towards warmer subtropical and tropical areas during warmer seasons. The statistically significant correlation between ACL and TAR with NGRIP d (Fig. 9) suggests that the atmospheric circulation responsible for environmental conditions in Western Europe was tightly linked with proposed circulation pattern, where during the first ~135 years of Greenland cooling warmer and moister air masses from the subtropical and tropical regions were reaching into Western Europe, particularly during the warmer seasons.

The common atmospheric system that can explain coherent atmospheric forcing on the Greenland precipitation moisture source areas from lower latitudes and Western Europe climate are the North Atlantic westerlies. We explain observed teleconnections through a progressive southwest-northeastern transition of the North Atlantic westerlies during the growing season for the first ~135 years of GS-1. We propose that the transition of the westerlies was caused by a progressive cooling and increase in the sea-ice

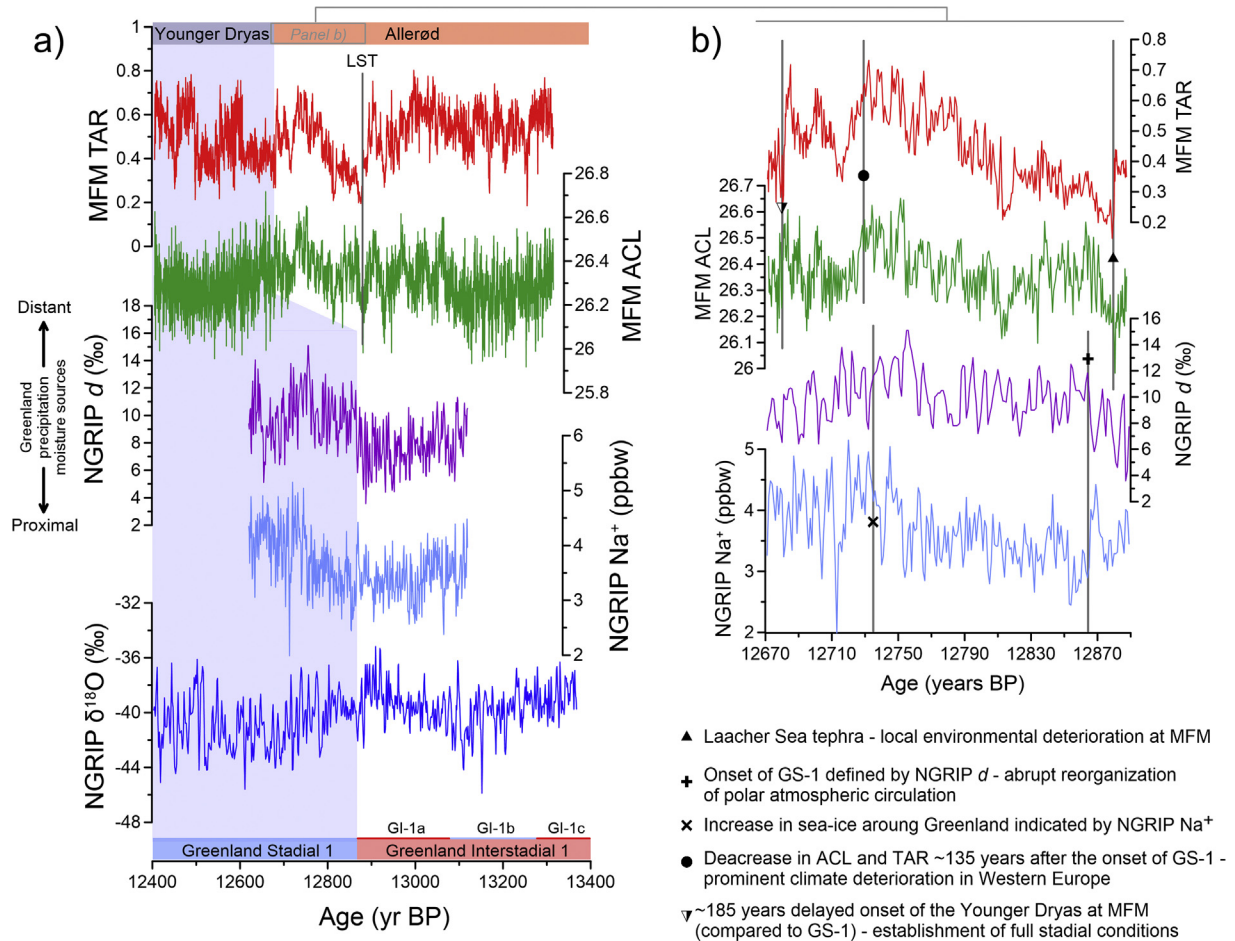


Fig. 8. Comparison of Meerfelder Maar and NGRIP. a) From top: comparison of Meerfelder Maar TAR (red line) and ACL (green line) with d (purple line), Na^+ (light blue line) and $\delta^{18}\text{O}$ (blue line) from NGRIP (Gkinis et al., 2014; Steffensen et al., 2008). Note that the NGRIP chronology is converted to the Meerfelder Maar chronology. Blue shaded areas indicate the onset of Greenland Stadial 1 in Greenland and the onset of the Younger Dryas in Western Europe. b) – zoom in the interval of time-transgressive onset of Greenland and Western Europe Younger Dryas cooling (indicated by a grey rectangle in the left panel).

extent over the Baffin Bay and Labrador Sea (west of Greenland) during the first ~135 years of GS-1, while the Norwegian Sea was sea-ice free and characterized by temporary return of warmer and more saline conditions (east of Greenland) (Muschiatiello and Wohlfarth, 2015; Muschiatiello et al., 2015). With a progressive cooling and increase in sea-ice west of Greenland, the polar front shifted to the south re-routing the westerlies over the western North Atlantic to the south. However, sea-ice east of Greenland was still limited during the onset of GS-1 (Muschiatiello and Wohlfarth, 2015; Muschiatiello et al., 2015) and the polar front did not reach its southern position as over the western North Atlantic at that time. This allowed the westerlies that were passing over low latitudes of the western North Atlantic to reach the higher latitudes of Western Europe during the growing season and prevent it from abrupt cooling, while Greenland was under stronger influence of the polar climate. Consequently, increase of the extent in the sea-ice and stronger polar front influence over the Labrador Sea was forcing a more southwest-northeastern westerlies route, progressively forcing warmer and moist air masses from the North Atlantic lower latitudes (subtropics and tropics) to reach Europe during spring to autumn in the first ~135 years of GS-1.

To further test the hypothesis that sea-ice positioning influenced the trajectory of warmer air masses, we compared MFM data with the pollen data from Tagus mud patch from the southwestern Iberian margin (Naughton et al., 2019, Fig. 10). We note that the

correlation of Tagus mud patch and MFM chronologies is not as robust as the correlation between MFM and NGRIP chronologies. Nevertheless, even when considering larger dating uncertainties, pollen data from the southern Iberian margin exhibit trends that resemble those of TAR and ACL from MFM during the time-transgressive onset of the Younger Dryas cooling (Fig. 10). In particular, a decrease in semi-desert and increase in heathland plants from 12,890 to 12,730 years BP indicates a progressive increase in moisture, whereas the increase in pine pollen suggest a contemporary increase in temperature (Naughton et al., 2019). At the same time, alkenone-based sea surface temperature (SST) from the same core (Naughton et al., 2019; Rodrigues et al., 2010) indicate a progressive sea surface cooling of up to 3 °C, suggesting that the southwestern Iberian margin climate was not directly controlled by North Atlantic SST but atmospheric circulation instead. We explain this by the proposed shift of the westerlies to the southwest-northeastern route, which passed over the southwestern Iberian margin and Western Europe, and influenced both regions in the same manner. Consequently, coherent environmental evolution of both regions further supports the proposed hypothesis and the increasing influence of warmer and moist air masses from the lower latitudes into Southwestern and Western Europe.

The first indication of Western Europe cooling is evident by a decrease in ACL and TAR at $\sim 12,730 \pm 40$ years BP (Figs. 6 and 8) and

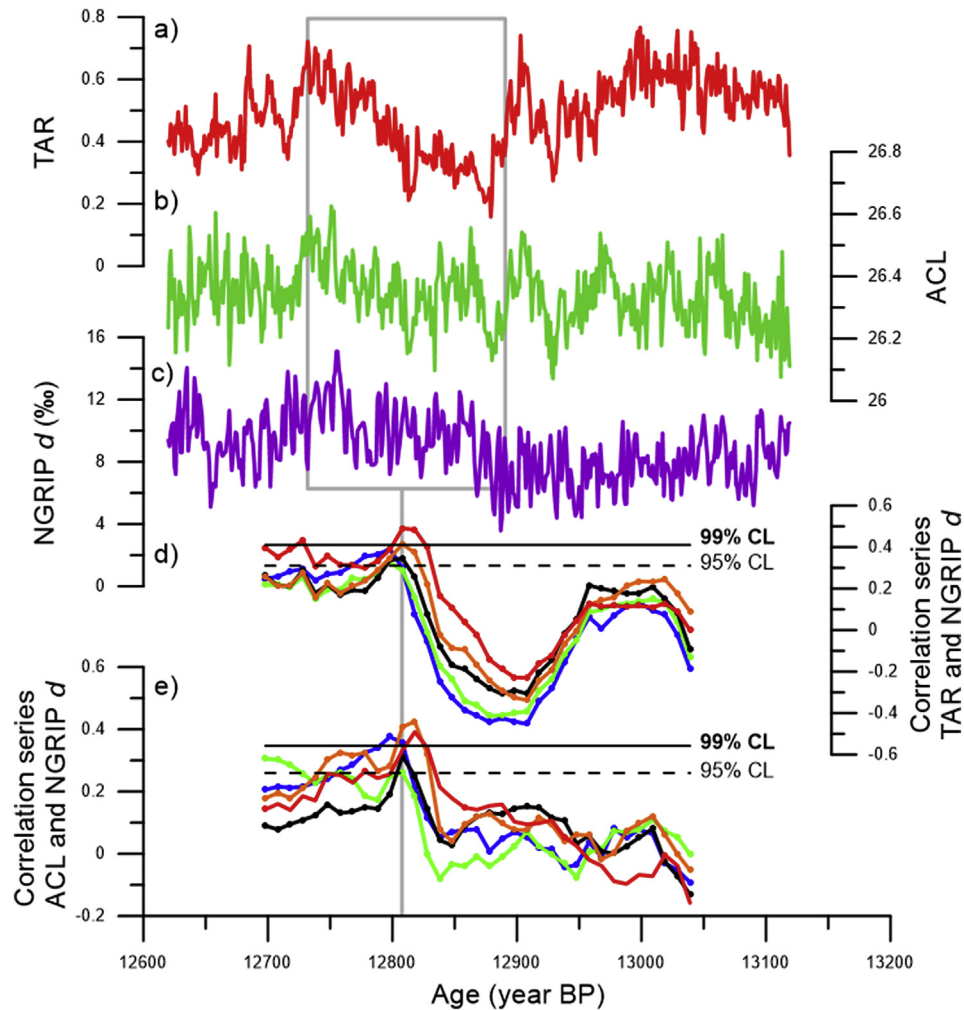


Fig. 9. Pearson correlation coefficient series for NGRIP d and TAR, and NGRIP d and ACL. Comparison of resampled TAR (a) and ACL (b) data-series on the sample grid of the NGRIP d data (i.e. 1-year resolution), with NGRIP d (c) and the correlation coefficient series among TAR and NGRIP d (d) and ACL and NGRIP d (e), as the result of 10-years sliding window approach with windows of 160-year width. Each point in time-series of correlation coefficient in (d) and (e) represent a middle of 160-years time window. For assuming robust correlation, five different age models were considered to account for ± 10 years uncertainty in converting NGRIP to MFM chronology (-10 (blue line), -5 (green line), 0 (black line), $+5$ (orange line) and $+10$ years (red line)). Both TAR and ACL show a significant correlation to NGRIP d record in the time period between 12,730–12,890 years BP (indicated by a grey rectangle; Supplementary Tables 2 and 3) and the correlation remains robust with age-model uncertainties. For visualization of different age models comparison with NGRIP d and corresponding correlation see Supplementary Fig. S4. Dashed lines in (d) and (e) represent 95% confidence level of correlation, while black lines represent 99% confidence level.

is further supported by a decrease in PAR (Engels et al., 2016) (Fig. 6) and the change in sedimentation regime (Engels et al., 2016). The decrease in heathland and pine vegetation pollen and the concurrent increase in semi-desert vegetation from Tagus mud patch reveal prominent aridification and cooling over the southwestern Iberian margin as well (Naughton et al., 2019, Fig. 10). We suggest that the observed climate change was imposed by an increased sea-ice cover over the Norwegian and North Seas (east of Greenland) (Muschiello et al., 2015), intensifying the polar front and triggering a southern shift of the westerlies also east of Greenland (Bakke et al., 2009; Isarin et al., 1998; Naughton et al., 2019). This is supported by an abrupt increase in NGRIP Na^+ data (Fig. 8); Na^+ data from NGRIP is a tentative proxy for sea-ice extent around Greenland where higher values indicated larger sea-ice extent (Schüpbach et al., 2018; Steffensen et al., 2008). The abrupt increase in sea-ice suggested by Na^+ roughly coincides with the prominent decrease of ACL and TAR values $\sim 12,730 \pm 40$ years BP (Fig. 8). Since the westerlies jet stream tends to separate colder, sub-polar air masses in the north from warmer, sub-tropical air masses in the south, a southward shift in the westerlies resulted in

the increased influence of the sub-polar climate over Western Europe. In addition, such wind trajectory was passing over the ice-covered North Atlantic carrying very dry air masses, reducing the heat transport to Western Europe. The suggested shift of the westerlies to the south due to increase in sea-ice and stronger polar front influence is consistent with Southern Europe tree-rings stable isotope records suggesting the stronger influence of North Atlantic air masses when compared to the Mediterranean air masses after $\sim 12,740$ years BP (Pauly et al., 2018).

Although we report initiation of vegetation response to cooling and aridification of Western Europe ~ 135 years after the onset of GS-1, the onset of Younger Dryas is defined at $12,680 \pm 40$ years BP (Litt and Stebich, 1999) (~ 185 years after the onset of GS-1). This suggests that regional environmental response to initiation of cooling caused by major storm track reorganization demanded about half a century for the establishment of full stadial conditions in Western Europe. We highlight a need to address this time-transgressive cooling in the future state of the art climate models, where high-resolution climate model simulations should test the proposed forcing mechanisms.

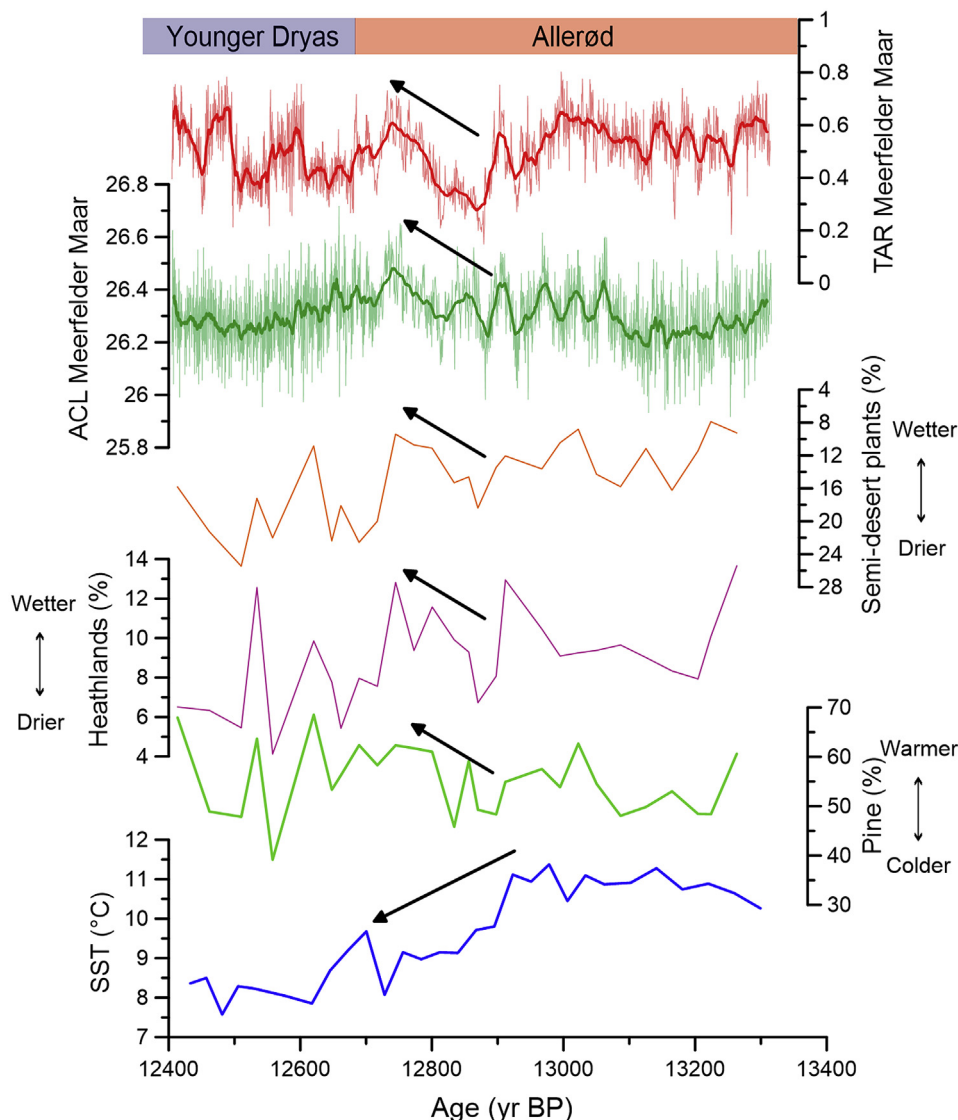


Fig. 10. Comparison of TAR and ACL data from Meerfelder Maar with pollen and SST records from Tagus mud patch (Naughton et al., 2019). TAR (red line) and ACL (green line) are in the top, while the pollen data from core D13882 are in the following order: semi-desert plants (orange line), heathlands (purple line) and pine (green line) vegetation. The pollen samples of pine are expressed as percentages of the total pollen sum, while pollen samples of semi-desert plants and heathlands are expressed as percentages calculated based on the main pollen sum (Naughton et al., 2019). At the bottom, an SST (blue line) record based on alkenones from core D13882 (Naughton et al., 2019; Rodrigues et al., 2010) is presented. Arrows indicate a common trend between TAR and ACL from MFM and pollen records from Tagus mud patch between 12,890 and 12,730 years BP, as well as opposing trend of the alkenone-based SST from Tagus mud patch.

4. Conclusion

In this study, we presented ultra-high-resolution molecular stratigraphy of fatty acids from Meerfelder Maar covering the Allerød-Younger Dryas transition. Fatty acid data support previous observation that major cooling and aridification of Western Europe lagged abrupt cooling in Greenland. However, we were able to demonstrate a statistically significant correlation between fatty acid data and NGRIP d on the ~annual scale at this time-transgressive period, suggesting that despite different climatic responses between Greenland and Western Europe, a common atmospheric forcing between Greenland precipitation source area and Western Europe was in place. We suggest a major reorganization in the North Atlantic westerlies amplified by the asynchronous increase in sea-ice and the polar front influence over the North Atlantic as a potential common forcing mechanism for time-

transgressive Younger Dryas cooling over the North Atlantic realm. However, proposed forcing mechanisms responsible for complex climate evolution of the North Atlantic realm at the onset of the Younger Dryas should be further tested due to the remaining ambiguity of sources of the analyzed fatty acids.

Acknowledgements

The investigations were carried out in the frame of the ZOOM-molecular project funded by the European Research Council (ERC) under the European Union's Horizon 2020 research and innovation programme (grant agreement No 670115, PI K.-U.H.). This study is a contribution to the Helmholtz-Association climate initiative REKLIM, Topic 8 "Rapid Climate Change from Proxy data". The published data are archived and available in the PANGAEA data repository (doi.pangaea.de/10.1594/PANGAEA.901468).

Appendix A. Supplementary data

Supplementary data to this article can be found online at <https://doi.org/10.1016/j.quascirev.2020.106198>.

References

- Alfken, S., Wörmer, L., Lipp, J.S., Wendt, J., Taubner, H., Schimmelmann, A., Hinrichs, K.-U., 2019. Micrometer scale imaging of sedimentary climate archives – sample preparation for combined elemental and lipid biomarker analysis. *Org. Geochem.* 127, 81–91.
- Baddouh, M., Meyers, S.R., Carroll, A.R., Beard, B.L., Johnson, C.M., 2016. Lacustrine $^{87}\text{Sr}/^{86}\text{Sr}$ as a tracer to reconstruct Milankovitch forcing of the Eocene hydrologic cycle. *Earth Planet Sci. Lett.* 448, 62–68.
- Bakke, J., Lie, Ø., Heegaard, E., Dokken, T., Haug, G.H., Birks, H.H., Dulski, P., Nilsen, T., 2009. Rapid oceanic and atmospheric changes during the Younger Dryas cold period. *Nat. Geosci.* 2, 202–205.
- Bechtel, A., Schubert, C.J., 2009. A biogeochemical study of sediments from the eutrophic Lake Lugano and the oligotrophic Lake Brienz. *Switz. Org. Geochem.* 40, 1100–1114.
- Bergström, I., Mäkelä, S., Kankaala, P., Kortelainen, P., 2007. Methane efflux from littoral vegetation stands of southern boreal lakes: an upscaled regional estimate. *Atmos. Environ.* 41, 339–351.
- Björck, S., Bennike, O., Rosén, P., Andresen, C.S., Bohncke, S., Kaas, E., Conley, D., 2002. Anomalously mild Younger Dryas summer conditions in southern Greenland. *Geology* 30, 427–430.
- Bligh, E.G., Dyer, W.J., 1959. A rapid method of total lipid extraction and purification. *Can. J. Biochem. Physiol.* 37, 911–917.
- Blockley, S.P.E., Bourne, A.J., Brauer, A., Davies, S.M., Hardiman, M., Harding, P.R., Lane, C.S., MacLeod, A., Matthews, I.P., Pyne-O'Donnell, S.D.F., et al., 2014. Tephrochronology and the extended intimate (integration of ice-core, marine and terrestrial records) event stratigraphy 8–128 ka b2k. *Quat. Sci. Rev.* 106, 88–100.
- Bodelier, P.L.E., Bär Gillisen, M.-J., Hordijk, K., Sinnighe Damsté, J.S., Rijpstra, W.I.C., Geenevasen, J.A.J., Dunfield, P.F., 2009. A reanalysis of phospholipid fatty acids as ecological biomarkers for methanotrophic bacteria. *ISME J.* 3, 606–617.
- Bourbonniere, R.A., Meyers, P.A., 1996. Sedimentary geolipid records of historical changes in the watersheds and productivities of Lakes Ontario and Erie. *Limnol. Oceanogr.* 41, 352–359.
- Bowman, J.P., Skerratt, J.H., Nichols, P.D., Sly, L.I., 1991. Phospholipid fatty acid and lipopolysaccharide fatty acid signature lipids in methane-utilizing bacteria. *FEMS Microbiol. Lett.* 85, 15–21.
- Brauer, A., Andres, C., Negendank, J.F.W., 1999a. Lateglacial calendar year chronology based on annually laminated sediments from Lake Meerfelder Maar, Germany. *Quat. Int.* 61, 17–25.
- Brauer, A., Andres, C., Günter, C., Litt, T., Stebich, M., Negendank, J.F.W., 1999b. High resolution sediment and vegetation responses to Younger Dryas climate change in varved lake sediments from Meerfelder Maar, Germany. *Quat. Sci. Rev.* 18, 321–329.
- Brauer, A., Haug, G.H., Dulski, P., Sigman, D.M., Negendank, J.F.W., 2008. An abrupt wind shift in western Europe at the onset of the Younger Dryas cold period. *Nat. Geosci.* 1, 520–523.
- Bush, R.T., McInerney, F.A., 2015. Influence of temperature and C_4 abundance on n -alkane chain length distributions across the central USA. *Org. Geochem.* 79, 65–73.
- Clement, A.C., Peterson, L.C., 2008. Mechanisms of abrupt climate change of the last glacial period. *Rev. Geophys.* 46.
- Conte, M.H., Weber, J.C., 2002. Plant biomarkers in aerosols record isotopic discrimination of terrestrial photosynthesis. *Nature* 417, 639–641.
- Denton, G.H., Alley, R.B., Comer, G.C., Broecker, W.S., 2005. The role of seasonality in abrupt climate change. *Quat. Sci. Rev.* 24, 1159–1182.
- Dyke, A.S., 2004. An outline of North American Deglaciation with emphasis on central and northern Canada. In: Ehlers, J., Gibbard, P.L. (Eds.), *Quaternary Glaciations: Extent and Chronology*. Elsevier Science and Technology Books, pp. 373–424.
- Ebisuzaki, W., 1997. A method to estimate the statistical significance of a correlation when the data are serially correlated. *J. Clim.* 10, 2147–2153.
- Elvert, M., Pohlman, J.W., Becker, K.W., Gaglioti, B., Hinrichs, K.-U., Wooller, M.J., 2016. Methane turnover and environmental change from Holocene lipid biomarker records in a thermokarst lake in Arctic Alaska. *Holocene* 26, 1766–1777.
- Engels, S., van Geel, B., Buddelmeijer, N., Brauer, A., 2015. High-resolution palynological evidence for vegetation response to the Laacher See eruption from the varved record of Meerfelder Maar (Germany) and other central European records. *Rev. Palaeobot. Palynol.* 221, 160–170.
- Engels, S., Brauer, A., Buddelmeijer, N., Martín-Puertas, C., Rach, O., Sachse, D., Geel, B. van, 2016. Subdecadal-scale vegetation responses to a previously unknown late-Allerød climate fluctuation and Younger Dryas cooling at Lake Meerfelder Maar (Germany). *J. Quat. Sci.* 31, 741–752.
- Gagosian, R.B., Peltzer, E.T., 1986. The importance of atmospheric input of terrestrial organic material to deep sea sediments. *Org. Geochem.* 10, 661–669.
- Gkinis, V., Simonsen, S.B., Buchardt, S.L., White, J.W.C., Vinther, B.M., 2014. Water isotope diffusion rates from the NorthGRIP ice core for the last 16,000 years – glaciological and paleoclimatic implications. *Earth Planet Sci. Lett.* 405, 132–141.
- Gong, C., Hollander, D.J., 1997. Differential contribution of bacteria to sedimentary organic matter in oxic and anoxic environments, Santa Monica Basin. *Calif. Org. Geochem.* 26, 545–563.
- Grafenstein, U. von, Erlenkeuser, H., Brauer, A., Jouzel, J., Johnsen, S.J., 1999. A mid-European decadal isotope-climate record from 15,500 to 5000 Years B.P. *Science* 284, 1654–1657.
- Grimalt, J.O., Yruela, I., Saiz-Jimenez, C., Toja, J., de Leeuw, J.W., Albaigés, J., 1991. Sedimentary lipid biogeochemistry of an hypereutrophic alkaline lagoon. *Geochem. Cosmochim. Acta* 55, 2555–2577.
- Gu, G., Dickens, G.R., Bhatnagar, G., Colwell, F.S., Hirasaki, G.J., Chapman, W.G., 2011. Abundant Early Palaeogene marine gas hydrates despite warm deep-ocean temperatures. *Nat. Geosci.* 4, 848–851.
- Hinrichs, K.-U., Hmelo, L.R., Sylva, S.P., 2003. Molecular fossil record of elevated methane levels in Late Pleistocene coastal waters. *Science* 299, 1214–1217.
- Hou, J., Huang, Y., Wang, Y., Shuman, B., Oswald, W.W., Faison, E., Foster, D.R., 2006. Postglacial climate reconstruction based on compound-specific D/H ratios of fatty acids from Blood Pond, New England. *Geochem. Geophys. Geosystems* 7.
- Huang, Y., Shuman, B., Wang, Y., Webb, T., 2002. Hydrogen isotope ratios of palmitic acid in lacustrine sediments record late Quaternary climate variations. *Geology* 30, 1103–1106.
- Huang, Y., Shuman, B., Wang, Y., Webb, T., 2004. Hydrogen isotope ratios of individual lipids in lake sediments as novel tracers of climatic and environmental change: a surface sediment test. *J. Paleolimnol.* 31, 363–375.
- Hughen, K.A., Eglinton, T.I., Xu, L., Makou, M., 2004. Abrupt tropical vegetation response to rapid climate changes. *Science* 304, 1955–1959.
- Isarin, R.F.B., Renssen, H., Vandenberghe, J., 1998. The impact of the north atlantic ocean on the younger Dryas climate in northwestern and central Europe. *J. Quat. Sci.* 13, 447–453.
- Ishiwatari, R., Yamamoto, S., Shinoyama, S., 2006. Lignin and fatty acid records in Lake Baikal sediments over the last 130 kyr: a comparison with pollen records. *Org. Geochem.* 37, 1787–1802.
- Kankaala, P., Käkki, T., Mäkelä, S., Ojala, A., Pajunen, H., Arvola, L., 2005. Methane efflux in relation to plant biomass and sediment characteristics in stands of three common emergent macrophytes in boreal mesoeutrophic lakes. *Global Change Biol.* 11, 145–153.
- Kelly, M.A., Lowell, T.V., Hall, B.L., Schaefer, J.M., Finkel, R.C., Goehring, B.M., Alley, R.B., Denton, G.H., 2008. A 10Be chronology of lateglacial and Holocene mountain glaciation in the Scoresby Sund region, east Greenland: implications for seasonality during lateglacial time. *Quat. Sci. Rev.* 27, 2273–2282.
- Kohn, M.J., 2010. Carbon isotope compositions of terrestrial C_3 plants as indicators of (paleo)ecology and (paleo)climate. *Proc. Natl. Acad. Sci. Unit. States Am.* 107, 19691–19695.
- Lane, C.S., Brauer, A., Blockley, S.P.E., Dulski, P., 2013. Volcanic ash reveals time-transgressive abrupt climate change during the Younger Dryas. *Geology* 41, 1251–1254.
- Lane, C.S., Brauer, A., Martín-Puertas, C., Blockley, S.P.E., Smith, V.C., Tomlinson, E.L., 2015. The Late Quaternary tephrostratigraphy of annually laminated sediments from Meerfelder Maar, Germany. *Quat. Sci. Rev.* 122, 192–206.
- Lauterbach, S., Brauer, A., Andersen, N., Danielopol, D.L., Dulski, P., Hüls, M., Milecka, K., Namiotko, T., Obremka, M., Grafenstein, U.V., 2011. Environmental responses to Lateglacial climatic fluctuations recorded in the sediments of pre-Alpine Lake Mondsee (northeastern Alps). *J. Quat. Sci.* 26, 253–267.
- Lehndorff, E., Wolf, M., Litt, T., Brauer, A., Amelung, W., 2015. 15,000 years of black carbon deposition – a post-glacial fire record from maar lake sediments (Germany). *Quat. Sci. Rev.* 110, 15–22.
- Litt, T., Stebich, M., 1999. Bio- and chronostratigraphy of the lateglacial in the Eifel region, Germany. *Quat. Int.* 61, 5–16.
- Lohne, Ø.S., Mangerud, J., Birks, H.H., 2013. Precise 14C ages of the Vedde and Saksunarvatn ashes and the Younger Dryas boundaries from western Norway and their comparison with the Greenland Ice Core (GICC05) chronology. *J. Quat. Sci.* 28, 490–500.
- Lotter, A.F., Eicher, U., Siegenthaler, U., Birks, H.J.B., 1992. Late-glacial climatic oscillations as recorded in Swiss lake sediments. *J. Quat. Sci.* 7, 187–204.
- Lücke, A., Brauer, A., 2004. Biogeochemical and micro-facial fingerprints of ecosystem response to rapid Late Glacial climatic changes in varved sediments of Meerfelder Maar (Germany). *Palaeogeogr. Palaeoclimatol. Palaeoecol.* 211, 139–155.
- Martin-Puertas, C., Brauer, A., Dulski, P., Brademann, B., 2012. Testing climate-proxy stationarity throughout the Holocene: an example from the varved sediments of Lake Meerfelder Maar (Germany). *Quat. Sci. Rev.* 58, 56–65.
- Masson-Delmotte, V., Jouzel, J., Landais, A., Stievenard, M., Johnsen, S.J., White, J.W.C., Werner, M., Sveinbjörnsdóttir, A., Fuhrer, K., 2005. GRIP deuterium excess reveals rapid and orbital-scale changes in Greenland moisture origin. *Science* 309, 118–121.
- Mangerud, J., Aarseth, I., Hughes, A.L.C., Lohne, S., Ø. S., Skår, K., Sønstegeard, E., Svendsen, J.I., 2016. A major re-growth of the scandinavian ice sheet in western Norway during allerød-younger Dryas. *Quat. Sci. Rev.* 132, 175–205.
- Meyers, P.A., 1997. Organic geochemical proxies of paleoceanographic, paleolimnologic, and paleoclimatic processes. *Org. Geochem.* 27, 213–250.
- Meyers, S., Malinverno, A., Hinnov, L., Moron, V., 2018. Astrochron: A Computational Tool for Astrochronology.
- Muschitiello, F., Wohlfarth, B., 2015. Time-transgressive environmental shifts across northern Europe at the onset of the younger Dryas. *Quat. Sci. Rev.* 109, 49–56.

- Muschitiello, F., Pausata, F.S.R., Watson, J.E., Smittenberg, R.H., Salih, A.A.M., Brooks, S.J., Whitehouse, N.J., Karlatou-Charalampopoulou, A., Wohlfarth, B., 2015. Fennoscandian freshwater control on Greenland hydroclimate shifts at the onset of the Younger Dryas. *Nat. Commun.* 6, 8939.
- Naughton, F., Costas, S., Gomes, S.D., Desprat, S., Rodrigues, T., Sanchez Goñi, M.F., Renssen, H., Trigo, R., Bronk-Ramsey, C., Oliveira, D., et al., 2019. Coupled ocean and atmospheric changes during Greenland stadial 1 in southwestern Europe. *Quat. Sci. Rev.* 212, 108–120.
- North Greenland Ice Core Project Members, 2004. High-resolution record of Northern Hemisphere climate extending into the last interglacial period. *Nature* 431, 147–151.
- O'Leary, M.H., 1988. Carbon isotopes in photosynthesis. *Bioscience* 38, 328–336.
- Pauly, M., Helle, G., Miramont, C., Büntgen, U., Treydte, K., Reinig, F., Guibal, F., Sivan, O., Heinrich, I., Riedel, F., et al., 2018. Subfossil trees suggest enhanced Mediterranean hydroclimate variability at the onset of the Younger Dryas. *Sci. Rep.* 8, 13980.
- Pfahl, S., Sodemann, H., 2014. What controls deuterium excess in global precipitation? *Clim. Past* 10, 771–781.
- Rach, O., Brauer, A., Wilkes, H., Sachse, D., 2014. Delayed hydrological response to Greenland cooling at the onset of the Younger Dryas in western Europe. *Nat. Geosci.* 7, 109–112.
- Rach, O., Kahmen, A., Brauer, A., Sachse, D., 2017. A dual-biomarker approach for quantification of changes in relative humidity from sedimentary lipid D/H ratios. *Clim. Past* 13, 741–757.
- Rasmussen, S.O., Andersen, K.K., Svensson, A.M., Steffensen, J.P., Vinther, B.M., Clausen, H.B., Siggaard-Andersen, M.-L., Johnsen, S.J., Larsen, L.B., Dahl-Jensen, D., et al., 2006. A new Greenland ice core chronology for the last glacial termination. *J. Geophys. Res. Atmos.* 111.
- Renssen, H., Mairesse, A., Goosse, H., Mathiot, P., Heiri, O., Roche, D.M., Nisancioglu, K.H., Valdes, P.J., 2015. Multiple causes of the Younger Dryas cold period. *Nat. Geosci.* 8, 946–949.
- Riede, F., Bazylev, O., Newton, A.J., Lane, C.S., 2011. A Laacher See-eruption supplement to TephraBase: investigating distal tephra fallout dynamics. *Quat. Int.* 246, 134–144.
- Rodrigues, T., Grimalt, J.O., Abrantes, F., Naughton, F., Jose-Abel Flores, J.-A., 2010. The last glacial-interglacial transition (LGIT) in the eastern mid-latitudes of the North Atlantic: abrupt sea surface temperature change and sea level implications. *Quat. Sci. Rev.* 29, 1853–1862.
- Sachse, D., Radke, J., Gleixner, G., 2006. δD values of individual *n*-alkanes from terrestrial plants along a climatic gradient – implications for the sedimentary biomarker record. *Org. Geochem.* 37, 469–483.
- Sánchez Goñi, M.F., Landais, A., Cacho, I., Duprat, J., Rossignol, L., 2009. Contrasting intrainterstadial climatic evolution between high and middle North Atlantic latitudes: a close-up of Greenland Interstadials 8 and 12. *Geochem. Geophys. Geosystems* 10, Q04U04.
- Schenk, F., Väiranta, M., Muschitiello, F., Tarasov, L., Heikkilä, M., Björck, S., Brandefelt, J., Johansson, A.V., Näslund, J.-O., Wohlfarth, B., 2018. Warm summers during the Younger Dryas cold reversal. *Nat. Commun.* 9, 1634.
- Schüpbach, S., Fischer, H., Bigler, M., Erhardt, T., Gfeller, G., Leuenberger, D., Mini, O., Mulvaney, R., Abram, N.J., Fleet, L., et al., 2018. Greenland records of aerosol source and atmospheric lifetime changes from the Eemian to the Holocene. *Nat. Commun.* 9, 1476.
- Sepúlveda, J., Pantoja, S., Hughen, K.A., Bertrand, S., Figueroa, D., León, T., Drenzek, N.J., Lange, C., 2009. Late Holocene sea-surface temperature and precipitation variability in northern Patagonia, Chile (Jacaf Fjord, 44°S). *Quat. Res.* 72, 400–409.
- Sirocko, F., Dietrich, S., Veres, D., Grootes, P.M., Schaber-Mohr, K., Seelos, K., Nadeau, M.-J., Kromer, B., Rothacker, L., Röhner, M., et al., 2013. Multi-proxy dating of Holocene maar lakes and Pleistocene dry maar sediments in the Eifel, Germany. *Quat. Sci. Rev.* 62, 56–76.
- Steffensen, J.P., Andersen, K.K., Bigler, M., Clausen, H.B., Dahl-Jensen, D., Fischer, H., Goto-Azuma, K., Hansson, M., Johnsen, S.J., Jouzel, J., et al., 2008. High-resolution Greenland ice core data show abrupt climate change happens in few years. *Science* 321, 680–684.
- Sturt, H.F., Summons, R.E., Smith, K., Elvert, M., Hinrichs, K.-U., 2004. Intact polar membrane lipids in prokaryotes and sediments deciphered by high-performance liquid chromatography/electrospray ionization multistage mass spectrometry—new biomarkers for biogeochemistry and microbial ecology. *Rapid Commun. Mass Spectrom.* 18, 617–628.
- Summons, R.E., Jahnke, L.L., Roksandic, Z., 1994. Carbon isotopic fractionation in lipids from methanotrophic bacteria: relevance for interpretation of the geochemical record of biomarkers. *Geochem. Cosmochim. Acta* 58, 2853–2863.
- Terwilliger, V.J., Eshetu, Z., Disnar, J.-R., Jacob, J., Paul Adderley, W., Huang, Y., Alexandre, M., Fogel, M.L., 2013. Environmental changes and the rise and fall of civilizations in the northern Horn of Africa: an approach combining δD analyses of land-plant derived fatty acids with multiple proxies in soil. *Geochem. Cosmochim. Acta* 111, 140–161.
- Whiticar, M.J., 1999. Carbon and hydrogen isotope systematics of bacterial formation and oxidation of methane. *Chem. Geol.* 161, 291–314.
- Wörmer, L., Elvert, M., Fuchser, J., Lipp, J.S., Buttigieg, P.L., Zabel, M., Hinrichs, K.-U., 2014. Ultra-high-resolution paleoenvironmental records via direct laser-based analysis of lipid biomarkers in sediment core samples. *Proc. Natl. Acad. Sci. Unit. States Am.* 111, 15669–15674.
- Wörmer, L., Lipp, J.S., Hinrichs, K.-U., 2017. Comprehensive analysis of microbial lipids in environmental samples through HPLC-MS protocols. In: McGenty, T.J., Timmis, K.N., Nogales, B. (Eds.), *Hydrocarbon and Lipid Microbiology Protocols: Petroleum, Hydrocarbon and Lipid Analysis*. Springer, Berlin, Heidelberg, pp. 289–317.
- Wörmer, L., Wendt, J., Alfken, S., Wang, J.-X., Elvert, M., Heuer, V.B., Hinrichs, K.-U., 2019. Towards multiproxy, ultra-high resolution molecular stratigraphy: enabling laser-induced mass spectrometry imaging of diverse molecular biomarkers in sediments. *Org. Geochem.* 127, 136–145.
- Woszczyk, M., Bechtel, A., Gratzner, R., Kotarba, M.J., Kokociński, M., Fiebig, J., Cieśliński, R., 2011. Composition and origin of organic matter in surface sediments of Lake Sarbsko: a highly eutrophic and shallow coastal lake (northern Poland). *Org. Geochem.* 42, 1025–1038.
- Wulf, S., Ott, F., Słowiński, M., Noryskiewicz, A.M., Dräger, N., Martin-Puertas, C., Czymzik, M., Neugebauer, I., Dulski, P., Bourne, A.J., et al., 2013. Tracing the laacher see tephra in the varved sediment record of the trzechowskie palaeolake in central northern Poland. *Quat. Sci. Rev.* 76, 129–139.
- Xing, Y., Xie, P., Yang, H., Ni, L., Wang, Y., Rong, K., 2005. Methane and carbon dioxide fluxes from a shallow hypereutrophic subtropical Lake in China. *Atmos. Environ.* 39, 5532–5540.
- Zöller, L., Blanchard, H., 2009. The partial heat – longest plateau technique: testing TL dating of Middle and Upper Quaternary volcanic eruptions in the Eifel Area, Germany. *EG – Quat. Sci. J.* 58.